Precise Control of Single-phenanthrene Junction's Conductance

Alaa Al-Jobory (a.al-jobory@uoanbar.edu.iq)
University of Anbar https://orcid.org/0000-0002-8001-8010
Abdelkareem Al-Meshal
Qassim University
Zainelabideen Yousif Mijbil
Al Qasim Green University: Al-Qasim Green University

Research Article

Keywords: Phenanthrene, Substituents, DFT-NEGF-TB, Charge transport, Quantum interference

Posted Date: July 26th, 2021

DOI: https://doi.org/10.21203/rs.3.rs-661943/v1

Precise control of single-phenanthrene junction's conductance

Abdelkareem Al-Meshal[1†], Alaa A. Al-Jobory[2‡♣], Zainelabideen Yousif Mijbil[3§♣]

[1]Department of Physics, College of Science and Arts in El-Mithnab, Qassim University, Saudi Arabia

[2]Department of Physics, College of Sciences, University of Anbar, Anbar, Iraq

[3]Department of Chemistry and Physiology, Veterinary Medicine College, Al-Qasim Green University, Al-Qasim Town, Babylon Province, 51013, Iraq

[†]amshl@qu.edu.sa, [‡] a.al-jobory@uoanbar.edu.iq, [§] z.ymijbil0@gmail.com and zymijbil@vet.uoqasim.edu.iq

Abstract

The electronic transmission of fifteen potential configurations of single-phenanthrene junction has been theoretically investigated. The structures include para-para, para-meta, and meta-meta combined with phenyl pendant group and substituted nitrogen atom. The results show that the para-meta, which offers a tunable antiresonance in the HOMO-LUMO gap, is the most suitable for synthesizing nano-device. The antiresonance is susceptible (unsusceptible) to the heteromotif location at site four (five). Hence, our paper presents the appropriate hetero-motif conditions—type and location— to synthesize molecular devices with the desired electronic conductance. The study also deepen the understanding of the molecular conductance by demonstrating the active and inactive sites to create and tune antiresonances. It finally introduces the essential impact of connectivity, quantum interference, and aromaticity in controlling the conductance of single-phenanthrene junction.

Keywords: Phenanthrene; Substituents; DFT-NEGF-TB; Charge transport; Quantum interference.

1. Introduction

Molecular electronics have had the potentials [1] to achieve stable and efficient electronic components such as sensors, transistors, and data storages [2, 3]. With device dimensions comparable with the wavefunctions of the propagating electrons, quantum phenomena have strongly emerged [4]. The phenomena represent the interactions between the wavefunctions of the nano-device functional molecule, which refers to the central molecule in the electronic

♣ Corresponding author.
♣ Corresponding author.

junction that is responsible for the device characteristics, and the wavefunctions of electrons passing through. Meanwhile, prominent examples of the quantum phenomena are the destructive quantum interference (DQI) and constructive quantum interference (CQI) that appear in the benzene ring attached to two external leads. The benzene shows high (CQI), low (DQI), and high (CQI) electrical conductance states associate with para, meta, and ortho connections, respectively [5-9]. Hence, understanding and harnessing these QIs to achieve the aforementioned potentials require developing advanced experimental techniques [4, 10] and theoretical methods [11-14]. For instance, enhanced thermal properties of double quantum dots [15] have been captured and controlled using Fano resonance [16]. Moreover, electrochemical gating was used to improve charge transport through biphenyl, triphenyl, and hexaphenyl molecular junctions [17].

In this paper, we follow a different approach that depends on intercalating single or multiple chemical substituents into the same functional molecule [18] provided that the junction retains the same conformation. One possible candidate is the easily synthesized polyaromatic hydrocarbon (PAH) molecules such as phenanthrene. The phenanthrene is an appealing molecule due to its rigid and anti-rotation structure [19-21]. It affords low electronic thermal conductance ($<0.005\ K_B/h$) with ignorable phononic thermal conductance that both enhance its thermoelectric efficiency [22]. The phenanthrene also shows a superconcutance when it is doped with alkali metals [23, 24]. Therefore, in this paper, the phenanthrene was attached to two gold leads in para-para, para-meta, and meta-meta connectivities with one or two carbon atoms substituted with (linked to) nitrogen atom “dopant” (phenyl radical “side group”). Such substituent or side group variation generates 15 molecular structures that may lead to 15 conductance states.

Consequently, we used the density functional method (DFT), non-equilibrium Green’s function (NEGF) method, and nearest-neighbor tight-binding (TB) approach to investigate the electronic transmission of the phenanthrene’s fifteen configurations. The results show less than one order of magnitude difference between the para-para and meta-meta connectivities in the energy region between the highest occupied molecular orbital (HOMO) and the lowest unoccupied molecular orbital (LUMO). Such insignificant difference, ensuring stable conductance states, results from the variation in the path lengths. However, the para-meta configurations represent the most delicate and essential structures because they offer controllable conductance states. These states essentially rely on the substituents’ type and location; but, they merely depend on the bond strength between the substituents or the constituents. Hence, various commercial dopants can be

embedded in the phenanthrene to manipulate its electrical conductance precisely. Thus, non-highly purified molecules with less restricted controlling conditions would save expenses and efforts.

2. Results and discussion

Our paper aims to show how the electrical conductance of a single PAH molecule can be precisely adjusted. The work focuses on the phenanthrene's transmission susceptibility to the connectivities and heteromotifs. The functional phenanthrene was attached to two Au-leads through pyridyl-acetylene anchor groups on both sides, see the Methodology section. It was linked to the anchors with three connection patterns: para-para (pp), para-meta (pm), and meta-meta (mm). Besides, we either substituted nitrogen (N) atom or attached phenyl radical (C_6H_5) at sites X and Y with varied combinations, as shown in Figure 1. Each combination was referred to as an integer number placed next to the predefined acronyms of connectivities. Hence, the final number of the studied configurations was 15 with five combinations per each connectivity pattern.

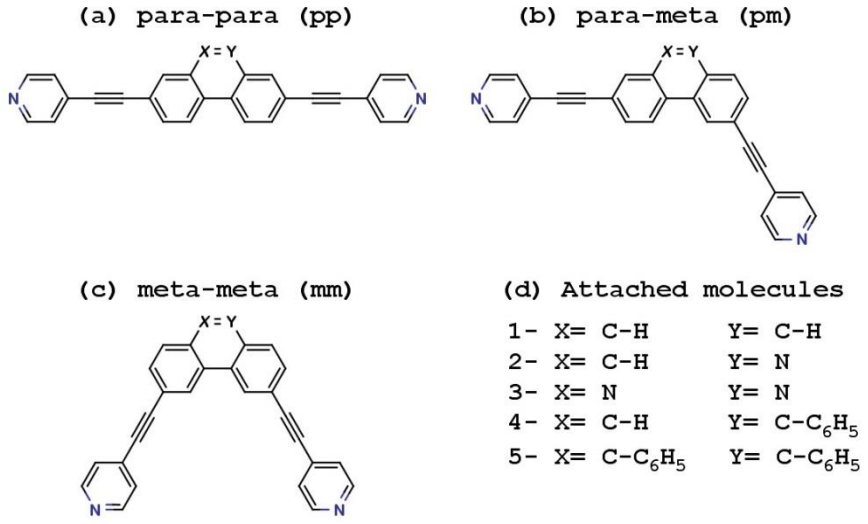

Figure 1. The phenanthrene molecule with (a) para-para, (b) para-meta, and (c) meta-meta connections to the pyridyl-acetylene anchor group. The (d) shows substituent motifs at X and Y locations.

The transmission coefficients of the fifteen structures, illustrated in Figure 2, raise one prominent and common feature, which is the coincidence of the Fermi level (E_F) (the vertical long-dashed line in Figure 2) with LUMO. The concurrence of the Fermi at LUMO is mainly due to the electron-withdrawing pyridyl anchor group [25, 26] that lowers the energy of the frontier orbitals and decreases the energy difference between the LUMO and the Fermi level [27]. When the BPB is attached to the Au-electrodes, the interaction between BPB and the external Au leads results from the bond between the antibonding π orbital of the pyridine and the Au *p*-orbital. This π^* represents the closest frontier orbital (LUMO) to electrode Fermi level [28]. Experimentally, Quek et al. showed that the conductance of 4,4'-bipyridine molecule attached to two gold electrodes is also LUMO dominated with high and low conductance states due to the bipyridine-gold conformation [29]. However, our transmission data presents one conductance states because the geometries between the gold and the adjacent pyridyl were fixed to focus on the electronic characteristics of the molecule only.

In addition to the Fermi level, the HOMO-LUMO energy range cannot be overlooked because it defines the chemical reactivity of the molecule [30-33]. Hence, scanning the HOMO-LUMO energy gap reveals similar and dissimilar behaviors among the studied lattices. The first result is the disappearance of the anti-resonance in the para-para (Figure 2a) and meta-meta (Figure 2c) with no anti-resonances. In contrast, anti-resonances manifest in the transmissions of the five asymmetric para-meta ones, Figure 2b. One route to rationalizing the results is to focus on the functional molecule alone by excluding the influence of the metalic leads and anchor groups. The exclusion is justified by the junctions' identical sides [34]. Besides, the 15 configurations were fully optimized in the gas phase under the same relaxation conditions. As a result, all junctions have the same Au-N separation distance (2.3 Å), the same location at the leads' top Au-atom, the same acetylene-phenanthrene distance (1.41 Å), and the same phenanthrene-pyridyl dihedral angle (0^o), accept for the phenyl-embraced phenanthrene (approximately 2^o=1.11% change). As the phenanthrene retains planar structure in all the 15 identical junctions, connectivity and substituent motifs were the only factors left to induce the anti-resonances in the para-meta connectivity. The solution to the appearance and disappearance of the anti-resonance lies in Figure 2b, where an anti-resonance is associated with the pristine phenanthrene, pm1 black curve. This curve proves the intrinsic occurrence of anti-resonance due to para-meta connectivity. The figure also depicts that each substituent results in a particular DQI location.

Hence, one can conclude that the connectivity generates the anti-resonance, and the hetero-motif tunes the location of the anti-resonance. The dependence of anti-resonance on connectivity has also been approved for hetero-aromatic hydrocarbons in our previous work [35]. So, these two factors control the quality of the electrical conductance of the molecule.

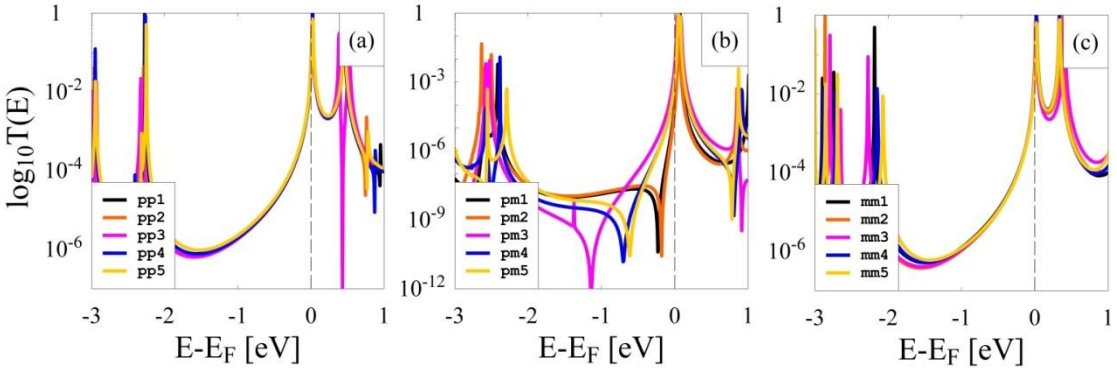

Figure 2. Electronic transmission of phenanthrene with (a) para-para, (b) para-meta, and (c) meta-meta connectivities. The long-dashed line illustrates the Fermi level (E_F).

A question now urges, *"why do the asymmetric para-meta structures alone show anti-resonances?*" The answer may appear from the QI graphical scheme of Markussen, Stadler, and Thygesen (MST), who suggested Hückel-based diagrammatic rules that analytically correlate QI to the molecular topology [34, 36], see section 3.3 in the Methodology. Applying the MST scheme to the TB models, we found a continuous line connecting the input site to the output site for all structures (the bold blue line in Figure 3). In addition, pairs of bonded sites (depicted by blue elliptic in Figure 3) have appeared. However, the para-meta case alone illustrates an isolated atomic site, called an onsite loop and shaded by a blue circle in Figure 3. The continuous line and atomic pairs permit the flowing of the electrons in contrast to the onsite loop that turns off the molecules. The conductance inhibition happens when the Green function element, describing the relation between the incoming and outgoing sites, goes to zero. Such a result implies that the onsite loop refers to phase shifting between the superposed electronic de Broglie waves passed along different paths through the molecule. Consequently, the two waves cancel out each other leading to destructive interference in the HOMO-LUMO energy range [37]. It is worth mentioning that Garner, Solomon, and Strange (GSS) published a similar paper that tracked the influence of the substituents on the electrical conductance of benzene and naphthalene. They

have also suggested a slightly developed MTS approach by relating the anti-resonance energy to the substituent onsite energy [18]. However, their anti-resonance correlation to the substituent onsite energy is inapplicable to the phenanthrene because they related the transmission coefficient to all possible paths that electrons may take to flow from one end to the other. Such procedure contradicts the DFT and TB calculations, for it shows that the pp and mm connectivities of phenanthrene could manifest anti-resonances near Fermi level, as shown in the three samples in the rightmost column in Figure 3. Therefore, this paper limits the applicability of Garner's team suggested method. To avoid distracting, we put all possible graphs according to the GSS scheme in Figure S1.

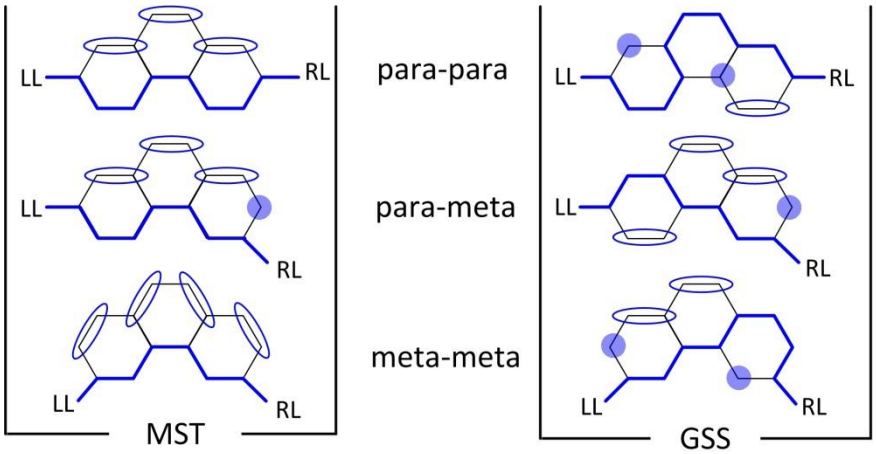

Figure 3. The MST (left column) and GSS (right column) graphical rules for electron transport through phenanthrene. The LL and RL respectively stand for the left and right leads.

Although the GSS scheme is inappropriate to our molecules, it encapsulates the anti-resonance dependence on the heteroatoms. Figure 2b not only associates the anti-resonance with the connectivity but also correlates it with the hetero-motifs. The compounds shift the anti-resonance relative to the Fermi level depending on the number and type of the included hetero-motifs. Here, the molecules should be divided into two groups: (i) compounds with one substituent or one pendant and those with (ii) two substituents or two pendants. The discrimination allows having a systematic study by focusing on a single variable rather than mixing up between two variables—the type and the number of motifs. Accordingly, the shifting of the anti-resonances

energy away from the Fermi of the two-hetero-motif embraced molecules follows the sequence: pristine (pm1) < 2×phenyl (pm5) < 2×N (pm3), and the shifting energy of the one-hetero-motif embraced molecules takes the order N (pm2) < phenyl (pm4). A close looking at these sequences reveals the strong influence of electronegativity on the anti-resonance location. Based on the Pauling scale, the electronegativity increases in the sequence H_{pm1} (2.2) < C_{pm5} (2.55) < N_{pm3} (3.04). Hence, it can be concluded that increasing the electronegativity of the hetero-motifs or the pendants will push the anti-resonance away from E_F toward the HOMO provided that we have two hetero-motifs or pendants [38-40]. The impact of the electronegativity was also reported in the work of Gantenbein *et al.* for para- and meta-anchored biphenyls [41] and Chen *et al.* [39]. The phenanthrene behaves differently when a single hetero-atom or pendent is added at site five, as shown in Figure 2b. First, the anti-resonance energy difference between the single nitrogen-incorporated phenanthrene and pristine phenanthrene is tiny ($\Delta E = 0.044$ eV). Secondly, the shifting of single phenyl is higher than the single nitrogen in opposite to the double-motif cases. Thirdly, the single phenyl's anti-resonance energy excels the double phenyls by 0.095 eV. Before preceding, one should remember that the polyaromatic phenanthrene consists of a central benzene molecule fused to two aromatic sextets [42]. Besides, the heterocyclic pyridine molecule resembles the benzene but with a single substituted nitrogen atom and less aromaticity. Hence, implementing one nitrogen atom in the phenanthrene would retain the same aromatic molecule with less aromaticity due to the nitrogen electronegativity, and it would preserve the charges within the molecule [43]. Thus, adding a high electronegative nitrogen atom will shift the anti-resonance toward the LUMO by withdrawing charges from the nearest C atom (site 4 in the TB). Charge variation of the carbon atom (site 4) is the crucial factor for antiresonance shifting of the single nitrogen, as shown in Figure 4f. In addition, the TB calculations, illustrated Figure 4c, show that varying the electronegativity of site five alone is surprisingly irresponsible for changing the anti-resonance location. On the other hand, the single nitrogen scenario is inapplicable for the phenyl ring because it is a pendant group, not an annealed motif. Consequently, the phenyl slightly withdraws charges out of the backbone phenanthrene so that it affects not only the adjacent carbon atom but also the total charge distribution of the central ring. When the phenyl ring depletes electrons from carbon atoms (4 and 5), it pushes the anti-resonance away from the LUMO. Unlike the single nitrogen atom which decreases the aromaticity and keeps the charges inside, the phenyl pulls charges outside and increases the

phenanthrene aromaticity, cf. table 12 in Ref. [44]. The aromaticity of the phenanthrene with single phenyl spreads charge deficiency all over the central benzene ring. Adding a second phenyl group to site four does not pull extra charges outside the phenanthrene, as we have only two exposable carbon atoms, as shown in Figure 4f. Our DFT charge populations support such behavior by showing that the single phenyl and double phenyls respectively pulled 0.03333 electron and 0.03575 electron from phenanthrene. Thus, the phenanthrene with 2-phenyls is more positive than the phenanthrene with 1-phenyl by approximately 6.76 percent.

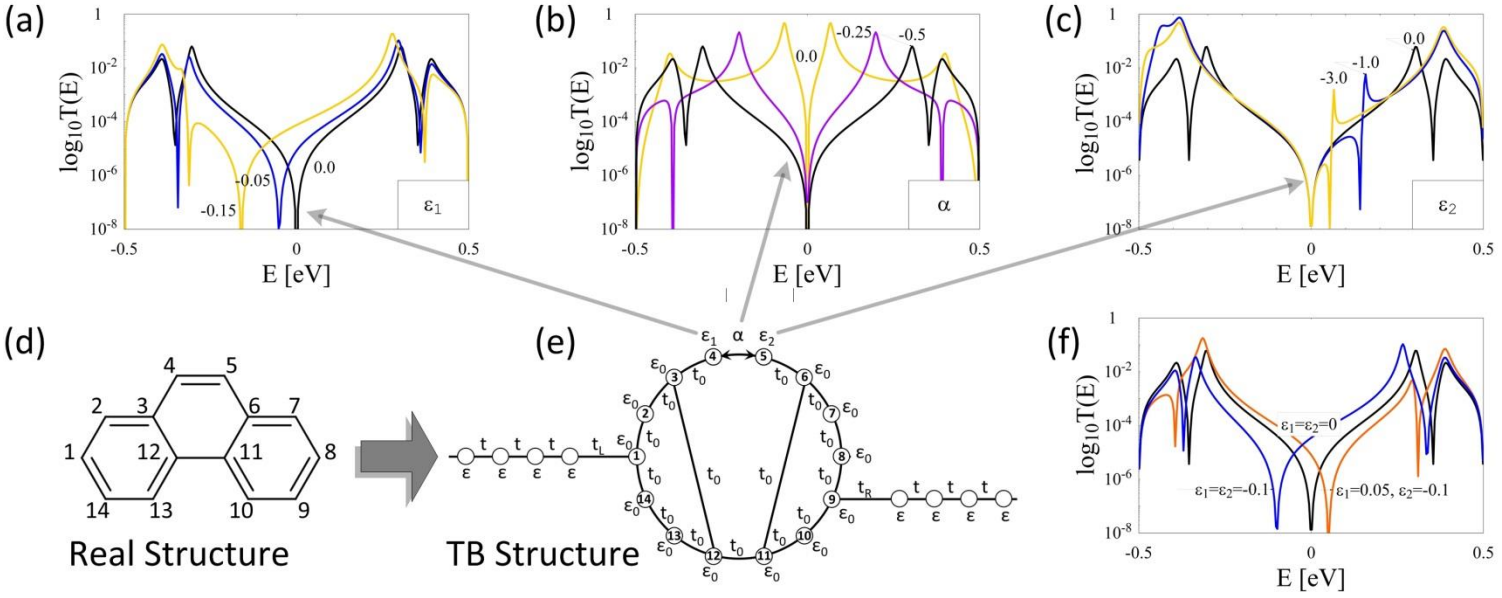

Figure 4. Tight binding transmission coefficient of para-meta connected phenanthrene. Panels (a), (b) and (c) respectively show the transmission variation with the onsite energy (ε_1) of the first modified site, bond strength (α) between the two modified sites, and the onsite energy (ε_2) of the second modified site. Panels (d) and (e) show the real and TB structures of phenanthrene molecule, respectively. Note: the values of ε_2 are order of magnitude higher than the values ε_1 to obtain an easy to understand behavior.

One approach to understanding the phenanthrene behavior is the nearest neighbor TB model. Hence, the realistic pp, pm, and mm molecular connectivities were respectively transformed into 1-8, 1-9, and 14-9 TB ones, illustrated in Figure 4. The general model assumes two left and right one-dimensional semi-infinite leads attached to the phenanthrene by the coupling integrals t_L=-0.3 eV and t_R=-0.3 eV, respectively. The two leads have the same onsite energies (ε=0.0 eV) and resonance integrals (t=-1.0 eV). The central system has the following parameters: onsite energy

ε_0=0.0 eV for the carbon-like sites, onsite energy ε_1 for the first modified site, onsite ε_2 for the second modified site, resonance integral t_0=-0.5 eV connecting any two nearest neighbors in the molecule except ε_1 and ε_2 that they were connected to each other by α. The pristine case of phenanthrene was envisaged by setting ε_0= ε_1= ε_2=0.0 eV, and t_0=α=-0.5 eV. The increased electronegativity of the sites was implemented in the TB models by increasing the negative value of the related onsite. Increasing the negative (positive) values of the onsite energy means an electron-withdrawing (donating) site. The TB results, Figure 4, show that the onsite energy of the substituents or pendants could essentially moderate the quantity and quality of the system's electronic transmission. Furthermore, the anti-resonance at the Fermi level of the pristine TB phenanthrene model in the pm connectivity supports the influence of the connectivity on the occurrence of nodes in the transmission, as shown in Figure 4 when ε_1=0.0 eV. On the contrary, the bond strength between the two adjacent modified sites does not affect the position of the anti-resonance.

The other feature is the higher electron transport of the pp junctions compared to the mm counterparts, see Figure 5. The transport curve also reflects the electronic density of states (DOS). Hence, the pp junctions possess higher DOS than the mm due to the different path lengths. Our DFT optimization shows shorter pp junctions (2.546 nm) than the mm ones (2.584 nm). The junction length is the distance between the top atoms of the two gold leads. Hence, the pp length is the direct virtual line connecting the two gold atoms; whereas, the mm length was divided into three sections. The first is defined by the distance between the top-gold-lead atom and the phenanthrene carbon atom attached to the linker. The second region is the direct distance between the two phenanthrene carbon atoms connected to the the adjacent linkers. The last region is confined by atoms 14, 4, and 9, as shown in Figure 4c. We first averaged the distances of region two and region three, and we summed the averaged distance with the length of the first section.

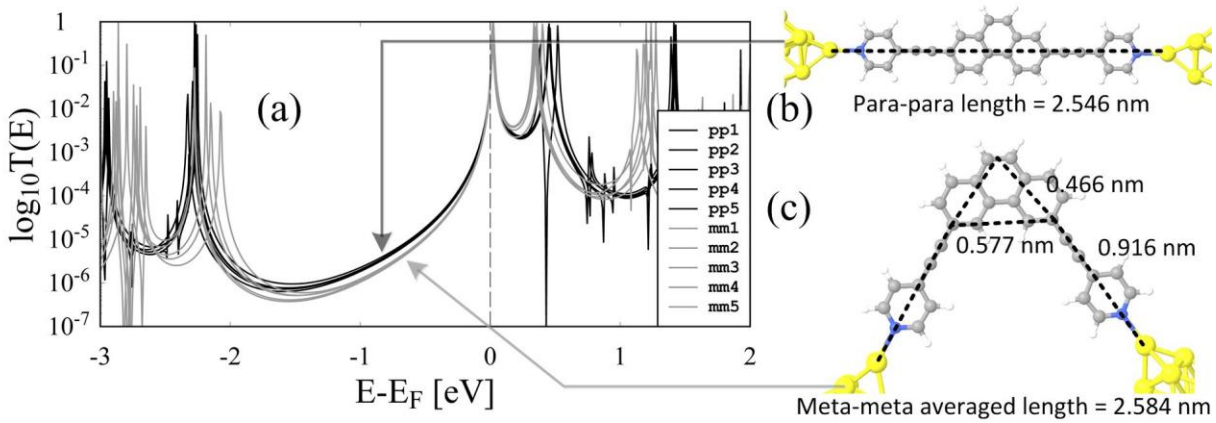

Figure 5. A comparison between all para-para (black lines) and all meta-meta (gray lines) connectivities of phenanthrene. Fermi level was represented by the vertical long-dashed line. The left panels show the length of the pp junction (b) and mm junction (c).

In real life, recent decades have witnessed the development of the experimental techniques to synthesize PAH with different heteroatoms [45, 46]. It is common now to replace one or more carbon atoms in the pristine PAH with single or multiple heteroatoms, but also attaching pendant molecules and controlling the twisting angling between the added molecule and the original functional molecule [19, 47-49]. For example, boron and nitrogen atoms can be replaced in the phenanthrene to tune its electrical conductance [50]. Furthermore, Venkataraman *et al.* investigated the dihedral angle between the functional PAH molecule and the attached side groups [19]. Numerous studies have shown that a single molecule can have multiple conductance states depending on the substituted heteroatoms. A prominent illustration is cyclopentadiene that possesses four conductance states associate with the type of the incorporated heteroatom [39, 40, 51]. Consequently, our results show the promising role of phenanthrene as a highly controllable building block for nano-electronic devices.

3. Theoretical Methods

3.1. Density Functional Theory

Quantum chemistry package, SIESTA [48], was implemented to obtain the ground state geometries of the molecules in the gas-phase. We used PBE version of GGA for the exchange and correlation effects [49], double zeta polarized basis sets for the phenanthrene and the anchor

group, double zeta basis sets for the gold leads, norm-conserving pseudopotentials for the core electrons [50], and 200 Ry for the real space grid cut-off energy. When the inter-atom forces were less than 40 meV/A, the systems were considered fully optimized. Furthermore, the optimum separation distance (2.3 Å) between the Au-leads the molecule was determined by finding the lowest binding energy between the two systems when they have rigidly shifted away from each other [51]. The final step was calculating the mean-field Hamiltonians of the whole junctions after fixing the geometry of the junction (metal-anchor group-molecule-anchor group-metal).

3.2. Electron transport

We calculated the phase-coherent electron transport of each system by implementing the DFT mean-field Hamiltonians into Gollum [52]. Gollum calculates the transmission coefficient $T(E)$ by applying the non-equilibrium Green function (NEGF) method using the following formula: $T(E) = trace(\Gamma_R(E)G^r(E)\Gamma_L(E)G^a(E))$. Where $G^r = 1/(ES - H - \Sigma_L - \Sigma_R)$ is the retarded GF, $G^a = G^{r^\dagger}$ is the advanced GF, $\Gamma_{L,R} = i(\Sigma_{L,R}(E) - \Sigma^\dagger_{L,R}(E))$ defines the broadening of energy levels of the molecule due to the coupling to the left (L) and right (R) leads, and $\Sigma_{L,R}$ are the retarded self-energies. Besides, GOLLUM utilizes the Landauer formula [53] in calculating electrical conductance, $G = G_0 \int dE\ T(E)\ (-\partial f_E(E))$. Furthermore, we used a simple tight-binding (TB) code Olife [54] to deal with nearest-neighbor TB models. Both Olife and Gollum exploit the same approximation; however, Olife is much easier code than Gollum especially with its build-in Graphical User Interface (GUI). It is worth mentioning that the reason for studying TB copies of the more realistic DFT structures is that the TB modes offer an initial and clear intuition about the behavior of the systems.

3.3. Markussen, Stadler, and Thygesen diagrammatic scheme

These three scientists suggested a diagram drawn on top of the molecule structure. This diagram refers to the path of the electrons traversing trough the molecule while they are flowing from the first lead to the second lead. The diagram also predicts the destructive or constructive interferences resulting from the interaction between the passing electrons' wavefunctions and the molecular orbitals wavefunctions. Besides, it represents a mathematical term in the retarded GF

(G'); in other words, the scheme provides an analytical description of the electron transport through the molecule near Fermi level. The MST diagrammatic scheme depends on two rules: (i) Only nearest neighbour sites are connected by a path, (ii) which has one input and one output ends over all sites except the first and final ones. Fulfilling these rules means continuous electron transport without destructive interferences and vice versa. Consequently, the transmission coefficient shows nodes when it has a disconnected path linking the sites 1 and N. The discontinuity occurs while the Green function goes to zero (G'=0). Hence, by adjusting the Fermi level to be zero [55, 56] so as the cure will be at the centre of the energy band, one can get

$$T(E_F = 0) \ \alpha \ G'_{1,N}(E_F = 0) \ \alpha \ \det_{1,N}(H_{molecule}) = 0,$$

where $T(E_F=0)$ is the transmission coefficient at Fermi level (E_F), $G'_{1,N}$ is the 1N matrix element of the retarded Green function, and $\det_{1,N}(H_{molecule})$ is the determinant of the molecule Hamiltonian excluding the 1st row and the Nth column.

4. Conclusions

Single phenanthrene ($C_{14}H_{10}$) molecule in pristine and doped with nitrogen and phenyl radical (C_6H_5) was attached in para-para (pp), meta-meta (mm), and para-meta (pm) connection to two gold leads. Hence, 15 configurations were analyzed using density functional theory (DFT), non-equilibrium Green function (NEGF), and nearest-neighbour tight-binding method (TB). The results illustrate similar trends of all para-para (mm) and meta-meta (mm) configurations. They have smooth electron transport in the HOMO-LUMO gap with no anti-resonances. Consequently, the pp and mm conductance states are higher than the pm although the electron transport of pp is slightly higher than mm. Even though anti-resonances in pm decrease the transmission coefficient, they allow more sovereignty over the junction electrical properties. Such control is accomplished by two factors: (i) the para-meta connectivity and (ii) type of the heteroatom and/or the pendent group. Hence, we believe that para-meta junction is more favourable for synthesizing of nanodevices due to the pm's applicable controlling factors that determine the junction electron transport.

Declaration

The authors declare no conflict of interests.

Author Contribution Statement:

All authors have given approval to the final version of the manuscript. All authors provided essential contributions to interpreting the data reported in this manuscript. Abdelkareem Al-Meshal: Software. Alaa A. Al-Jobory: Software, Conceptualization, Methodology, Formal analysis. Zainelabideen Y. Mijbil: Conceptualization, Methodology, Software, Analysis, Writing - Original Draft, Writing- Reviewing and Editing.

References

[1] A.A. Al-Jobory, M.D. Noori, Thermoelectric Properties of Metallocene Derivative Single-Molecule Junctions, Journal of Electronic Materials. 49 (2020) 5455-5459.

[2] B. Chen, K. Xu, Single Molecule-Based Electronic Devices: A Review, Nano. 14 (2019) 1930007.

[3] A.A. Al-Jobory, Z.Y. Mijbil, M. Noori, Tuning electrical conductance of molecular junctions via multipath Ru-based metal complex wire, Indian Journal of Physics. (2019).

[4] N. Xin, J. Guan, C. Zhou, X. Chen, C. Gu, Y. Li, M.A. Ratner, A. Nitzan, J.F. Stoddart, X. Guo, Concepts in the design and engineering of single-molecule electronic devices, Nature Reviews Physics. 1 (2019) 211-230.

[5] X. Li, Z. Tan, X. Huang, J. Bai, J. Liu, W. Hong, Experimental investigation of quantum interference in charge transport through molecular architectures, Journal of Materials Chemistry C. 7 (2019) 12790-12808.

[6] G. Yang, H. Wu, J. Wei, J. Zheng, Z. Chen, J. Liu, J. Shi, Y. Yang, W. Hong, Quantum interference effect in the charge transport through single-molecule benzene dithiol junction at room temperature: An experimental investigation, Chinese Chemical Letters. 29 (2018) 147-150.

[7] C.R. Arroyo, S. Tarkuc, R. Frisenda, J.S. Seldenthuis, C.H.M. Woerde, R. Eelkema, F.C. Grozema, H.S.J. van der Zant, Signatures of Quantum Interference Effects on Charge Transport Through a Single Benzene Ring, Angewandte Chemie International Edition. 52 (2013) 3152-3155.

[8] C.J. Lambert, Basic concepts of quantum interference and electron transport in single-molecule electronics, Chemical Society Reviews. 44 (2015) 875-888.

[9] J. Vahedi, Z. Sartipi, Effects of quantum interference on the electron transport in the semiconductor/benzene/semiconductor junction, Molecular Physics. 113 (2015) 1422-1432.

[10] T.A. Su, M. Neupane, M.L. Steigerwald, L. Venkataraman, C. Nuckolls, Chemical principles of single-molecule electronics, Nature Reviews Materials. 1 (2016) 1-15.

[11] Z.Y. Mijbil, Quantum interference in monocyclic molecules: A novel and straightforward phase wave model, Karbala International Journal of Modern Science. (2020).

[12] J. Lambert Colin, S.-X. Liu, A Magic Ratio Rule for Beginners: A Chemist's Guide to Quantum Interference in Molecules, Chemistry – A European Journal. 24 (2017) 4193-4201.

[13] D. Nozaki, S.M. Avdoshenko, H. Sevinçli, R. Gutierrez, G. Cuniberti, Prediction of quantum interference in molecular junctions using a parabolic diagram: Understanding the origin of Fano and anti- resonances, Journal of Physics: Conference Series. 427 (2013) 012013.

[14] A. Ismael, A. Al-Jobory, X. Wang, A. Alshehab, A. Almutlg, M. Alshammari, I. Grace, T.L.R. Benett, L.A. Wilkinson, B.J. Robinson, N.J. Long, C. Lambert, Molecular-scale thermoelectricity: as simple as 'ABC', Nanoscale Advances. 2 (2020) 5329-5334.
[15] J. Bai, Z. He, L. Li, S. Dang, Y. Li, W. Sun, The influence of side-coupled quantum dots on thermoelectric effect of parallel-coupled double quantum dot system, Physica B: Condensed Matter. 545 (2018) 377-382.
[16] G. Gómez-Silva, O. Ávalos-Ovando, M.L. Ladrón de Guevara, P.A. Orellana, Enhancement of thermoelectric efficiency and violation of the Wiedemann-Franz law due to Fano effect, Journal of applied physics. 111 (2012) 053704.
[17] N. Xin, X. Li, C. Jia, Y. Gong, M. Li, S. Wang, G. Zhang, J. Yang, X. Guo, Tuning charge transport in aromatic-ring single-molecule junctions via ionic-liquid gating, Angewandte Chemie. 130 (2018) 14222-14227.
[18] M.H. Garner, G.C. Solomon, M. Strange, Tuning Conductance in Aromatic Molecules: Constructive and Counteractive Substituent Effects, The Journal of Physical Chemistry C. 120 (2016) 9097-9103.
[19] L. Venkataraman, J.E. Klare, C. Nuckolls, M.S. Hybertsen, M.L. Steigerwald, Dependence of single-molecule junction conductance on molecular conformation, Nature. 442 (2006) 904.
[20] M.F. Christopher, S. Skon, W.B. Steven, M.G. Iain, M.G.-S. Víctor, J.L. Colin, Conformation dependence of molecular conductance: chemistry versus geometry, Journal of Physics: Condensed Matter. 20 (2008) 022203.
[21] D. Visontai, I.M. Grace, C.J. Lambert, Electron transport through ribbonlike molecular wires calculated using density-functional theory and Green's function formalism, Physical Review B. 81 (2010) 035409.
[22] M. Razeghi, S. Izadi Vishkayi, H. Rahimpour Soleimani, The effect of geometric arrangement on the thermoelectric properties of Phenanthrene coupled to the graphene nanoribbons electrodes, Chinese Journal of Physics. 56 (2018) 2580-2588.
[23] A.L. Pitman, J.A. McLeod, E. Khozeimeh Sarbisheh, E. Kurmaev, J. Müller, A. Moewes, X-ray Spectroscopic Study of the Conduction Band of K3:Anthracene and K3:Phenanthrene, The Journal of Physical Chemistry C. 117 (2013) 19616-19621.
[24] X.F. Wang, Y.J. Yan, Z. Gui, R.H. Liu, J.J. Ying, X.G. Luo, X.H. Chen, Superconductivity in $A_{1.5}$ phenanthrene (A = Sr,Ba), Physical Review B. 84 (2011) 214523.
[25] L. Sun, Y.A. Diaz-Fernandez, T.A. Gschneidtner, F. Westerlund, S. Lara-Avila, K. Moth-Poulsen, Single-molecule electronics: from chemical design to functional devices, Chemical Society Reviews. 43 (2014) 7378-7411.
[26] G. Yzambart, L. Rincón-García, A.A. Al-Jobory, A.K. Ismael, G. Rubio-Bollinger, C.J. Lambert, N.s. Agraït, M.R. Bryce, Thermoelectric Properties of 2, 7-Dipyridylfluorene Derivatives in Single-Molecule Junctions, The Journal of Physical Chemistry C. 122 (2018) 27198-27204.
[27] H.M. Osorio, S. Martín, M.C. López, S. Marqués-González, S.J. Higgins, R.J. Nichols, P.J. Low, P. Cea, Electrical characterization of single molecule and Langmuir–Blodgett monomolecular films of a pyridine-terminated oligo (phenylene-ethynylene) derivative, Beilstein Journal of Nanotechnology. 6 (2015) 1145-1157.
[28] M. Kamenetska, S.Y. Quek, A. Whalley, M. Steigerwald, H. Choi, S.G. Louie, C. Nuckolls, M. Hybertsen, J. Neaton, L. Venkataraman, Conductance and geometry of pyridine-linked single-molecule junctions, Journal of the American Chemical Society. 132 (2010) 6817-6821.
[29] S.Y. Quek, M. Kamenetska, M.L. Steigerwald, H.J. Choi, S.G. Louie, M.S. Hybertsen, J. Neaton, L. Venkataraman, Mechanically controlled binary conductance switching of a single-molecule junction, Nature Nanotechnology. 4 (2009) 230-234.
[30] T. Hansen, G.C. Solomon, D.Q. Andrews, M.A. Ratner, Interfering pathways in benzene: An analytical treatment, The Journal of Chemical Physics. 131 (2009) 194704.

[31] J.-i. Aihara, Correlation found between the HOMO–LUMO energy separation and the chemical reactivity at the most reactive site for isolated-pentagon isomers of fullerenes, Physical Chemistry Chemical Physics. 2 (2000) 3121-3125.
[32] S. Liu, Dynamic behavior of chemical reactivity indices in density functional theory: A Bohn-Oppenheimer quantum molecular dynamics study, Journal of Chemical Sciences. 117 (2005) 477-483.
[33] J.-i. Aihara, Reduced HOMO−LUMO Gap as an Index of Kinetic Stability for Polycyclic Aromatic Hydrocarbons, The Journal of Physical Chemistry A. 103 (1999) 7487-7495.
[34] T. Markussen, R. Stadler, K.S. Thygesen, The Relation between Structure and Quantum Interference in Single Molecule Junctions, Nano Letters. 10 (2010) 4260-4265.
[35] Z.Y. Mijbil, A.A. Al-Jobory, Tuning the Length-Dependent Conductance of Thiophene and Furan's Derivatives Via Connectivity, Journal of Electronic Materials. 49 (2020) 7457-7463.
[36] T. Markussen, R. Stadler, K.S. Thygesen, Graphical prediction of quantum interference-induced transmission nodes in functionalized organic molecules, Physical Chemistry Chemical Physics. 13 (2011) 14311-14317.
[37] P. Sautet, C. Joachim, Electronic interference produced by a benzene embedded in a polyacetylene chain, Chemical Physics Letters. 153 (1988) 511-516.
[38] Y. Yang, M. Gantenbein, A. Alqorashi, J. Wei, S. Sangtarash, D. Hu, H. Sadeghi, R. Zhang, J. Pi, L.-C. Chen, X. Huang, R. Li, J. Liu, J. Shi, W. Hong, C.J. Lambert, M.R. Bryce, Heteroatom-Induced Molecular Asymmetry Tunes Quantum Interference in Charge Transport through Single-Molecule Junctions, The Journal of Physical Chemistry C. 122 (2018) 14965−14970.
[39] W. Chen, H. Li, J.R. Widawsky, C. Appayee, L. Venkataraman, R. Breslow, Aromaticity decreases single-molecule junction conductance, Journal of the American Chemical Society. 136 (2014) 918-920.
[40] Z.Y. Mijbil, Electronegativity, symmetry, and bond strength intrinsically control charge transport through five-membered single-molecule junction, The European Physical Journal B. 92 (2019) 220.
[41] M. Gantenbein, L. Wang, A.A. Al-jobory, A.K. Ismael, C.J. Lambert, W. Hong, M.R. Bryce, Quantum interference and heteroaromaticity of para- and meta-linked bridged biphenyl units in single molecular conductance measurements, Scientific Reports. 7 (2017) 1794.
[42] R. Kalescky, E. Kraka, D. Cremer, Description of aromaticity with the help of vibrational spectroscopy: Anthracene and phenanthrene, The Journal of Physical Chemistry A. 118 (2014) 223-237.
[43] G.M. Loudon, Organic Chemistry, Oxford University Press, 2001.
[44] O. Martínez-Santiago, Y. Marrero-Ponce, S.J. Barigye, H. Le Thi Thu, F.J. Torres, C.H. Zambrano, J.L. Muñiz Olite, M. Cruz-Monteagudo, R. Vivas-Reyes, L. Vázquez Infante, Physico-chemical and structural interpretation of discrete derivative indices on N-tuples atoms, International journal of molecular sciences. 17 (2016) 812.
[45] H.-Y. Lv, G.-H. Zhong, M. Chen, C.-L. Yang, X.-J. Chen, H.-Q. Lin, Structure, charge transfer, and superconductivity of M-doped phenanthrene (M = Al, Ga, and In): A comparative study of K-doped cases, Science China Physics, Mechanics & Astronomy. 62 (2019) 957412.
[46] R. Mitsuhashi, Y. Suzuki, Y. Yamanari, H. Mitamura, T. Kambe, N. Ikeda, H. Okamoto, A. Fujiwara, M. Yamaji, N. Kawasaki, Y. Maniwa, Y. Kubozono, Superconductivity in alkali-metal-doped picene, Nature. 464 (2010) 76-79.
[47] W. Xu, E. Leary, S. Hou, S. Sangtarash, M.T. González, G. Rubio-Bollinger, Q. Wu, H. Sadeghi, L. Tejerina, K.E. Christensen, Unusual Length Dependence of the Conductance in Cumulene Molecular Wires, Angewandte Chemie. 131 (2019) 8466-8470.
[48] D. Vonlanthen, A. Mishchenko, M. Elbing, M. Neuburger, T. Wandlowski, M. Mayor, Chemically Controlled Conductivity: Torsion-Angle Dependence in a Single-Molecule Biphenyldithiol Junction, Angewandte Chemie International Edition. 48 (2009) 8886-8890.

[49] A. Mishchenko, D. Vonlanthen, V. Meded, M. Bürkle, C. Li, I.V. Pobelov, A. Bagrets, J.K. Viljas, F. Pauly, F. Evers, M. Mayor, T. Wandlowski, Influence of Conformation on Conductance of Biphenyl-Dithiol Single-Molecule Contacts, Nano Letters. 10 (2010) 156-163.

[50] Z.-H. Zhao, L. Wang, S. Li, W.-D. Zhang, G. He, D. Wang, S.-M. Hou, L.-J. Wan, Single-Molecule Conductance through an Isoelectronic B–N Substituted Phenanthrene Junction, Journal of the American Chemical Society. 142 (2020) 8068-8073.

[51] A. Borges, G.C. Solomon, Effects of Aromaticity and Connectivity on the Conductance of Five-Membered Rings, The Journal of Physical Chemistry C. 121 (2017) 8272-8279.

[52] J. Ferrer, C.J. Lambert, V.M. García-Suárez, D.Z. Manrique, D. Visontai, L. Oroszlany, R. Rodríguez-Ferradás, I. Grace, S.W.D. Bailey, K. Gillemot, S. Hatef, L.A. Algharagholy, GOLLUM: a next-generation simulation tool for electron, thermal and spin transport, New Journal of Physics. 16 (2014) 093029.

[53] R. Landauer, Spatial variation of currents and fields due to localized scatterers in metallic conduction, IBM Journal of Research and Development. 1 (1957) 223-231.

[54] Z.Y. Mijbil, OLIFE: Tight Binding Code for Transmission Coefficient Calculation, Journal of Physics: Conference Series. 1003 (2018) 012114.

[55] Z.Y. Mijbil, H.O. Essa, Destructive-quantum-interference suppression in crown ether single molecule junction, The European Physical Journal B. 93 (2020) 106.

[56] K. Lambropoulos, C. Simserides, Spectral and transmission properties of periodic 1D tight-binding lattices with a generic unit cell: an analysis within the transfer matrix approach, Journal of Physics Communications. 2 (2018) 035013.